THE UNIVERSITY OF MANITOBA

CONDUCTION HEAT TRANSFER IN A TUBULAR RESISTANCE HEATER WITH A HELICAL RESISTANCE COIL

by

J. R. Lion

A Thesis
Submitted to the Faculty of Graduate Studies
in Partial Fulfilment of the Requirements for the Degree
of Master of Science

Department of Mechanical Engineering

Winnipeg, Manitoba
September, 1975

"CONDUCTION HEAT TRANSFER IN A TUBULAR RESISTANCE HEATER WITH A HELICAL RESISTANCE COIL"

by

J. R. LION

A dissertation submitted to the Faculty of Graduate Studies of the University of Manitoba in partial fulfillment of the requirements of the degree of

MASTER OF SCIENCE

ABSTRACT

The design of electrical tubular resistance heaters has in the past been hampered by a lack of knowledge of resistance wire temperature as a function of geometry. This study provides a method of determining the conduction heat transfer between the helical resistance wire coil and the metal sheath material. From this the wire temperature may be calculated.

Shape factors for conduction from the wire to the sheath were found by using a finite element computer program which modeled each turn of the resistance wire helix as a torus of revolution. After computing shape factors for a wide range of geometries, the model was tested using an electrical analog technique.

Through the use of these predetermined shape factors, resistance wire temperature can be calculated for a particular geometry given only the sheath surface temperature, thermal conductivity of the insulating medium, and the watt density on the resistance wire.

ACKNOWLEDGEMENTS

I would like to thank Dr. G. K. Yuill for his guidance and encouragement throughout the course of this work. I would also like to acknowledge the assistance given by many other members of the Faculty of Engineering. In particular, gratitude is extended to Dr. T. R. Hsu and Mr. G. Bertels for their help in the computer analysis and to Dr. K. McLachlan and Dr. M. Chaturvedi for their help in the experimental study. Thanks also to Mr. L. E. Windsor and the staff of the Temro Division of James B. Carter Limited for their assistance. I would also like to acknowledge the Manitoba Research Council for the R.A.D.A.P. grant that made this study possible. Thanks are also due to Mrs. Jeanne Wright for her careful typing of this thesis. Last, but far from least, I would like to thank my wife, Donna, for her patience and understanding.

TABLE OF CONTENTS

LIST OF FIGURES

LIST OF TABLES

NOMENCLATURE

A	area
b	odds
d	diameter
D	dimensionless diameter
E	electrical potential
G	shape factor
h	convective heat transfer co-efficient
i	electrical current
K	thermal conductivity
L	length
m	mean
P	helix pitch
P	dimensionless pitch
Q	heat flux
R	electrical or thermal resistance
t	wall thickness of sheath material
T	temperature

Greek Symbols

ρ	electrical resistivity
Δ	difference
θ	helix lead angle
π	3.14

ℓ	length
ω	uncertainty·interval
v	independent variable

Subscripts

a	ambient or helix inside
i	inner
o	outer
s	surface or sheath
std	standard
w	wire

CHAPTER I

INTRODUCTION

1.1 Background Information

Since not everyone is familiar with the construction of electrical tubular resistance heaters, a brief outline of the processes and materials involved is presented. It is hoped that the reader will gain a clearer understanding of the main part of this presentation after reading this background material. However, this information is not intended as a precise description of all the different manufacturing techniques used. Rather, it is only a brief description of the general characteristics of a tubular resistance heater.

1.1.1 Basic Heater Description

An electric tubular resistance heater is composed of three basic parts; the resistance wire helix, the electrical insulating medium, and a tubular metal sheath.

Resistance wire is most commonly made from 80-20 nickel-chromium alloy with traces of iron and silicon. However, other resistance wire alloys are widely used; for example, alloys of chromium, aluminum, and iron.

The resistance wire helix must be protected

electrically by a non-conductor from the tubular metal sheath. This insulating material must have both high dielectric strength and good thermal conductance. Although other materials may be used for this purpose, granular magnesium oxide is most common.

The resistance wire helix and insulating material are enclosed in a thin walled metal tube of copper, stainless or mild steel, nickel alloys, aluminum, or other material, depending on the final application. The metal tubing provides protection against the environment and allows a means of increasing the density of the insulating material, the importance of which will be discussed below.

Figure (1.1) is a schematic of the components of an electrical tubular resistance heater.

1.1.2 Manufacturing Processes

The following is a brief description of the various stages in the manufacturing of an electrical tubular resistance heater.

The obvious first step in producing a heating element is its initial design. The main design criterion is the rate at which an element must produce heat to fit its final application. For a given voltage this is determined solely by the total electrical resistance of the resistance wire helix. As there are many ways of obtaining the required

FIGURE 1.1
SCHEMATIC OF AN ELECTRIC TUBULAR RESISTANCE HEATER

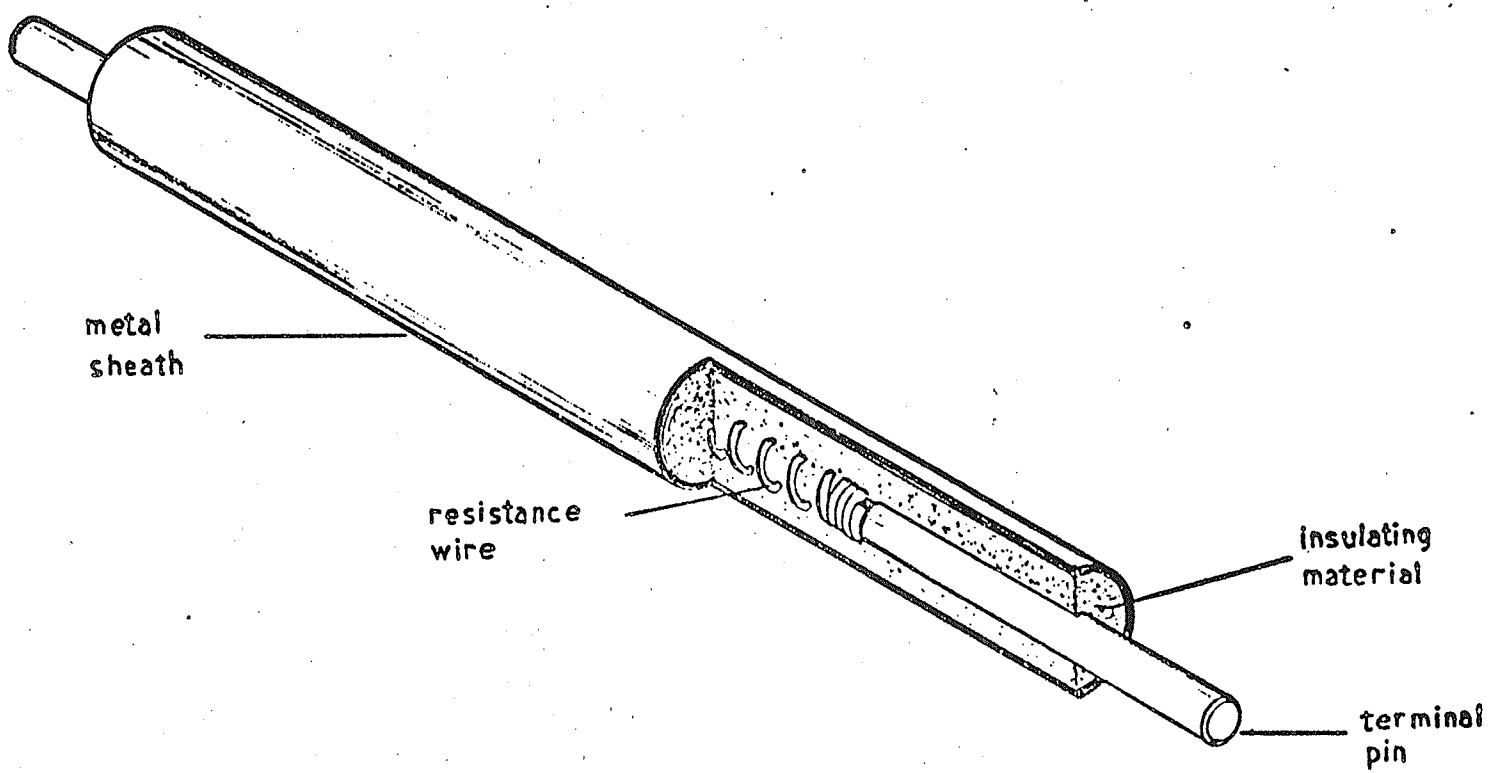

resistance, a specific geometry for heater construction must be chosen. The geometric variables of a heating element are; resistance wire diameter, arbor diameter, helix pitch, and heater element outside diameter. Then, before construction begins, other design decisions are made, such as; the length and type of terminal pins, overall heater length, and the type of sheath material.

The first construction process is that of winding the resistance wire into a helix of the required length. Winding may be done mechanically on a machine that draws the wire around a stationary cylinder into a continuous helix. The helix is then automatically cut to the desired length. Alternately, winding may be accomplished by turning a length of drill rod in a variable speed drill and manually feeding the the wire onto the rod. An ohmmeter may then be used to measure the desired electrical resistance therefore determining the helix length.

It should be noted that the helix now has a pitch equal to one wire diameter. That is, the helix is close wound with one turn touching another rather than stretched to a larger pitch as in the finished heater. The inside diameter is now the sum of the arbor diameter, the diameter of the cylinder on which it was wound, and the wire "springback". The springback is caused by the elasticity in the resistance wire and its effect is to cause the helix

to unwind somewhat. Thus the inside diameter of helix is slightly larger than the arbor cylinder diameter. This phenomenon usually causes an increase in diameter of only a few thousandths of an inch.

The next step in the production process is to fasten terminal pins to both ends of the helix. This may be done in various ways. One way is to push a number of turns of the helix around the cylindrical terminal pin and make a spot resistance weld, thus fusing the helix to the terminal pin. Another method is crimping the helix to the pin. Again a few turns of the helix are pushed over the end of the terminal pin. This assembly is then held in a die while a stamping operation deforms the wire thus fastening the helix to the terminal pin. Yet another method is to use threaded terminal pins and simply thread the helix onto the pin.

In the next production step, the helix and terminal pin assembly is held concentrically in a length of the metal tubing chosen for sheath material. The helix is stretched to a predetermined length so that the terminal pins protrude slightly from both ends of the tubing. Next the insulating medium is vibrated into the metal sheath and falls around the terminal pins as well as around and between the turns of the resistance wire helix. The helix and terminal pin assembly is thus electrically insulated from the metal sheath material. There are various ways of producing the above

configuration. Perhaps the most common is a batch process in which the helix and terminal pin assembly is held stationary on a machine. The length of metal tubing for sheath material is then mechanically moved down around the helix assembly and at the same time stretches the helix to its required length. The insulating medium, usually magnesium oxide, is then vibrated into the tubing. The vibration serves to increase the density of the magnesium oxide which results in a higher thermal conductance.

Thermal conductance increases exponentially with increasing density in most granular insulating materials used in heater elements. Since it is desirable to have as little thermal resistance as possible between the resistance wire helix and the tubular metal sheath, operations are performed to increase the density of the insulating medium. One way to achieve this is to draw the metal tube containing the insulating material through a set of rolls. For powdered magnesium oxide, a significant diameter reduction compresses the powder into a granular solid. At this point the tubular resistance heater is a straight cylinder with a work hardened metal sheath, the basic electrical tubular resistance heater.

1.2 Statement Of The Problem

The lack of knowledge of the maximum heat flux that may be prescribed for a particular geometry has hindered

designers of tubular heating elements. That is, what resistance wire or sheath watt density may be prescribed and still allow the resistance wire to remain at a temperature low enough to ensure a long heater service life.

Many problems are encountered in measuring resistance wire temperature. For example, thermocouple probes inserted into heating elements give limited accuracy since the measurement is only local. Furthermore, heat is conducted away through the thermocouple faster than through the insulating medium. Also the geometry of the heater may be easily disturbed by inserting the probe. F. S. Epstein (ref. 1) describes a method of determining resistance wire temperature by using the helix as a resistance thermometer. Although his method allows accurate determination of wire temperature for a particular heater, it does not enable the determination of a reuseable shape factor since the thermal conductivity of the insulating material remains unknown. Therefore, the scope of this approach is limited to single geometries and a single insulating material having a standard density.

1.3 Scope Of The Thesis

The study presented here utilized a simplified model of the resistance wire helix and a finite element computer analysis of the heat transfer. The model's geometry was varied, thereby simulating a wide range of tubular heating

elements. Shape factors were determined over a range of variables which covered most of the heater geometries commonly manufactured. Dimensionless variables were used in plotting the data to allow the user to easily identify the correct shape factor for the geometry in question.

The computer simulation was tested using a steady state electrical analog technique with a liquid conductor. This was found to be preferable to determining the shape factor from an actual heater because of the difficulty in accurately obtaining the thermal conductivity of the insulating medium. The analog measurements agreed well with the results found in the computer study.

CHAPTER II

COMPUTER SIMULATION

2.1 The Model

In order to compute the conduction heat transfer between the resistance wire helix and the outer sheath material, a simplified model was constructed. This model allowed solution by the numerical finite element technique.

Since there were four geometric variables, three of them were non-dimensionalized by dividing them by the wire diameter. The computed shape factor is presented as a function of these non-dimensionalized variables in sets of curves that cover the range of values encountered in common heater geometries.

2.1.1 Simplification

The resistance wire helix was modeled as a series of doughnut shaped elements or tori. Each turn of wire in the helix was modeled as a torus of revolution having helix inside diameter the same as the torus inside diameter. The pitch of the helix, the axial length for one turn of wire, was modeled as the center to center axial length between two adjacent tori. The wire diameter of the helix and torus circle diameter of the model were the same.

The outside diameter of the heating element, the sheath diameter, was the same in the torus model as it was in the real heater. Figures (2.1.1) and (2.1.2) illustrate the helix and the model described above.

As can be seen from Figure (2.1.2) the geometry becomes axisymmetric when modeled in this way. A single element has a disk shape such as would be made by rotating the wedge shown in Figure (2.2.1) to fill the entire 360^{o}. The volume normally filled by the resistance wire was omitted as will be explained below. Figure (2.2.2) shows an infinitesimally thin slice of the wedge shown in Figure (2.2.1). The dimensions, "p", "d_w", "d_a", and "d" fully describe a heater geometry when modeled as a series of tori of revolution.

2.1.2 Assumptions And Boundary Conditions

Heat flux and temperature boundary conditions were applied to the axisymmetric shape as shown in Figure (2.2.2).

In the torus model the temperature field is a function of the axial and radial co-ordinates and is not a function of the angular co-ordinate. Therefore, the adiabatic sides shown are found by symmetry from adjoining identical elements. The bottom of the element is obviously adiabatic since it is the axis of symmetry.

The resistance wire was assumed isothermal since its

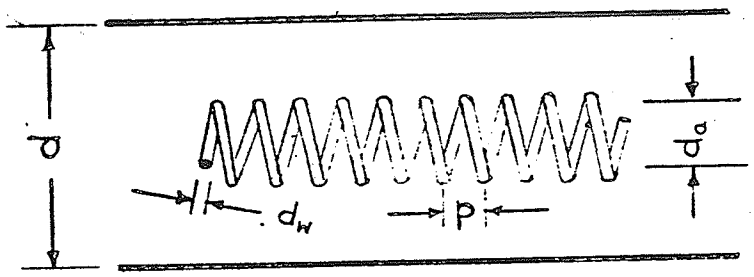

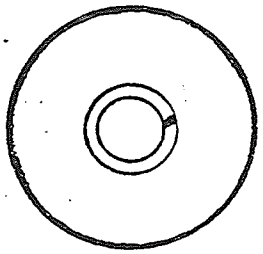

d — heater outside diameter
d_a — helix inside diameter
d_w — wire diameter
p — pitch

FIGURE 2.1.1

HELIX AS IN ACTUAL HEATER

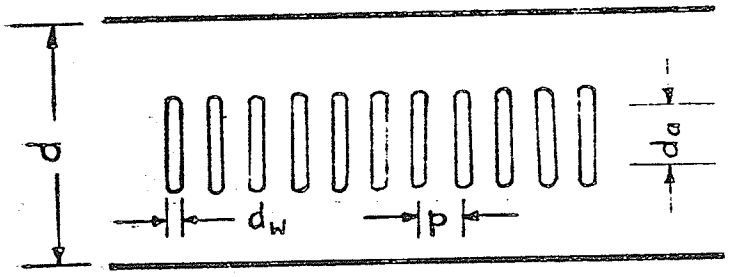

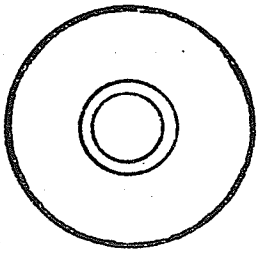

FIGURE 2.1.2

TORUS MODEL

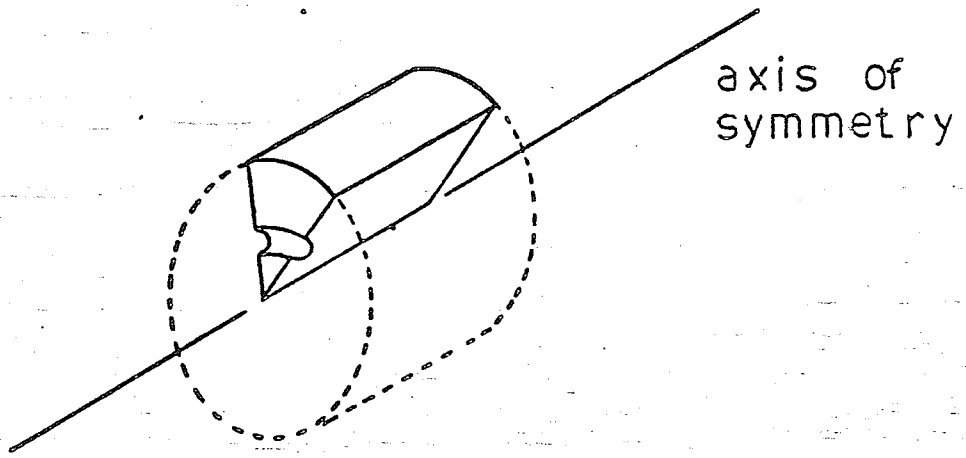

FIGURE 2.2.1
ELEMENTAL VOLUME

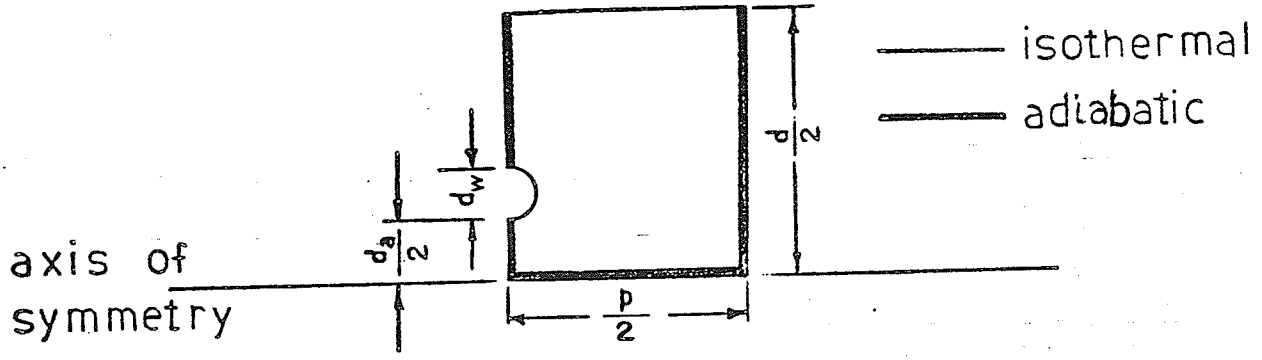

FIGURE 2.2.2
COMPUTER MODEL

thermal conductivity is fifty to one hundred times greater than that of the electrical insulating material. This assumption was further verified by a finite element computer analysis in which the resistance wire was part of the elemental volume. The resistance wire was assumed to have uniform heat generation. It was found that the temperature differences between any two points in the resistance wire were negligible. Therefore, the semi-circular region shown in Figure (2.2.2) was considered isothermal.

For similar reasons the comparatively thin layer of sheath material was not included as part of the grid for the final computer program. Common sheath materials such as copper and mild steel have thermal conductivities fifty to four hundred times greater than that of the electrical insulating material. A preliminary finite element analysis showed that the sheath material was nearly isothermal in both axial and radial directions. The absence of the sheath material in the elemental volume also greatly simplified the manipulation of input for the computer program because the elemental volume was composed of one material only.

2.1.3 Changing Geometry

The basic finite element grid which was drawn on the shape shown in Figure (2.2.2), is presented in Figure (2.3). As numerous heater geometries were studied various alterations were made to the basic grid to accommodate particular geometries. For example, for larger arbor diameters blocks of insulating material had to be added to the bottom of the shape shown in Figure (2.3). Similarly, for larger heater outside diameters blocks of insulating material were added to the top of the grid. To allow for changes in pitch or stretch ratio of the helix, insulating material was added in the axial direction. A computer program was written to produce punched input data for the many different geometries. Since the grid contained a single material, obtaining computer run input data for the varied geometries was accomplished with comparative ease.

2.1.4 Computer Program

The finite element computer program, "NLHEAT", that was used for this study was developed by Hsu and Bertels (ref. 2), using a method described by Wilson and Nickell, (ref. 3).

The computer program was flexible and handled both axisymmetric and planar geometries. It allowed the speci-

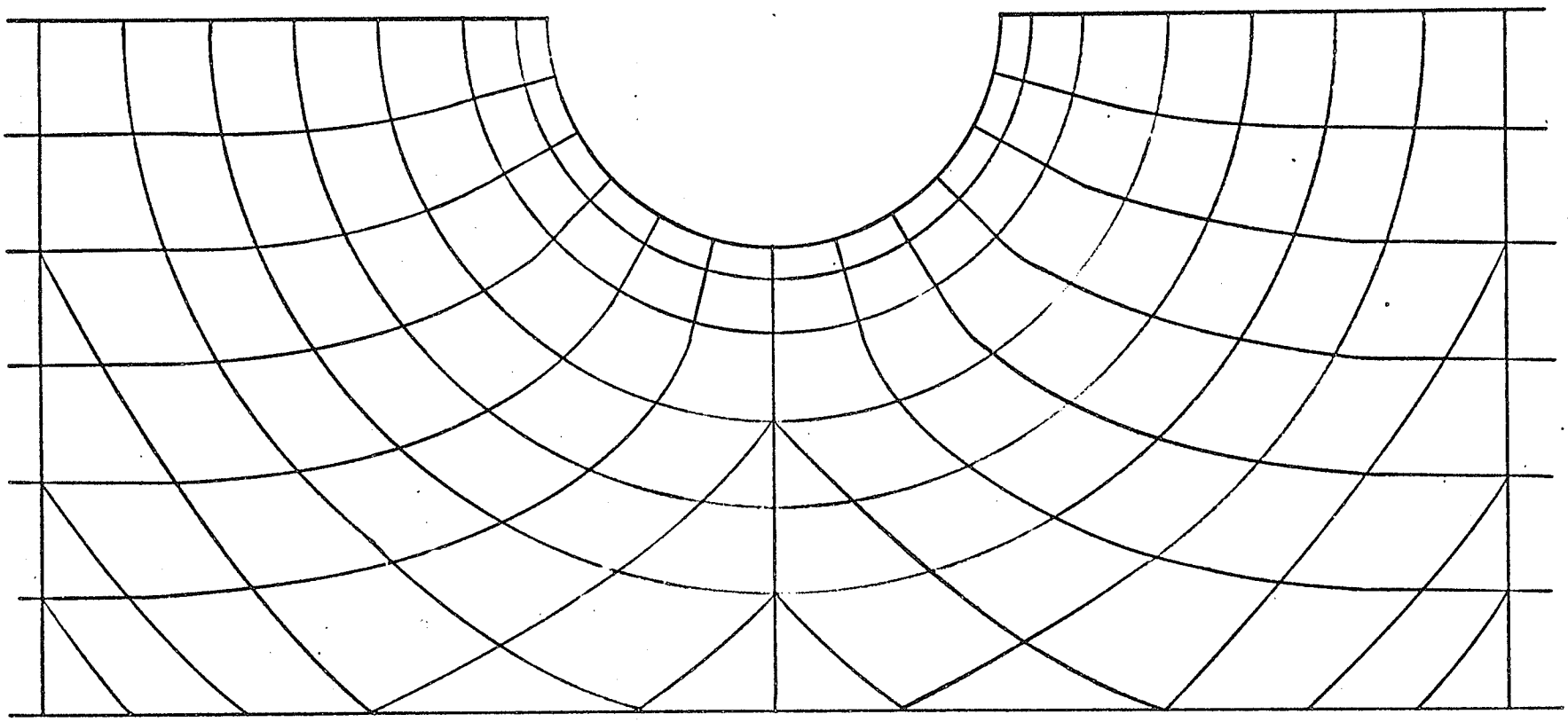

FIGURE 23
FINITE ELEMENT GRID

fication of isothermal and adiabatic boundaries. Material properties and heat transfer co-efficients could be made to vary with temperature, time, and position. The computer program calculated and returned node point temperatures for any specified set of conditions.

For the torus model the following set of specifications or boundary conditions were applied. Referring again to Figure (2.2.2), the semi-circular boundary representing the wire surface was given a prescribed temperature. The upper horizontal boundary which represents the outer surface of the heating element was given a prescribed uniform convective heat transfer co-efficient. In the case of the adiabatic boundaries, there was no prescribed heat transfer co-efficient and, therefore, no heat could be transferred through those boundaries. The insulating material was given a uniform thermal conductivity which was approximately the value of thermal conductivity of compacted magnesium oxide found in heating elements. As previously mentioned, a preliminary analysis showed that even for a heater with a large helix inside diameter and a convective heat transfer co-efficient of 1 Btu./ft.^{2} - hr. - ^oF, the outer surface of the heater was found to be isothermal within two degrees Fahrenheit.

Before using the computer program on the torus model, it was checked for accuracy by using known geometries such

as the plane wall and concentric cylinder. It was found that the numerical solution compared to five significant figures with the exact analytical solution.

Several different grid sizes were used when the torus model was analyzed. It was found that enlarging the grid size did not significantly change the computer results for the same geometry.

2.1.5 Calculating A Shape Factor

The method used to determine a single shape factor from the results of the computer program was as follows:

A shape factor describes the influence of geometry between two isothermal surfaces in heat conduction problems. Since the resistance wire was modeled as an isothermal surface and the outside heater surface was found to be almost isothermal from computer results, the use of shape factors was feasible. The conduction equation for this case is:

$$Q = G K (T_W - T_S) \quad \ldots\ldots\ldots \quad 2.1$$

where

Q = heat loss (Btu./hr.)

G = shape factor (ft.)

K = thermal conductivity of insulating material (Btu./hr. - ft. - ^{o}F)

T_w = resistance wire temperature prescribed in computer program (^oF)

T_s = surface or sheath temperature calculated by the computer program (^oF)

In equation 2.1, G is the shape factor having units of length and is equal to a representative area divided by a representative length. The shape factor is a function of geometry only.

Since this is a steady state heat transfer process, the total heat flux from the resistance wire is equal to the total heat flux from the heater surface for the elemental volume shown in Figure (2.2.1). The surface heat loss is given by:

$$Q = h_s A (T_s - T_a) \quad \ldots\ldots\ldots \quad 2.2$$

where

h_s = convective heat transfer co-efficient prescribed in the computer program (Btu./hr. - ft.^{2} - ^oF)

T_a = ambient temperature prescribed in the computer program (^oF)

A = heater surface area (ft.^{2})

The area, A, for the torus model is equal to the product of the circumference and half the pitch.

The shape factor, G, per unit axial length of heater can then be found by rearranging equation 2.1 to the form:

$$G = \frac{Q}{\frac{1}{2} p K (T_w - T_s)} \quad \ldots\ldots\ldots \quad 2.3$$

where

p = is the axial pitch between two adjacent tori (ft.)

and evaluated by substituting the value of Q from equation 2.2. Equation 2.3 is divided by ½ p because the elemental volume under consideration has that axial length as shown in Figure (2.2.2).

2.2 Results Of The Computer Study

In this section the results of the computer study are presented. A sample calculation is also presented to indicate how these results may be used on a real heater.

2.2.1 Presentation Of The Data

Over five hundred computer runs were made to encompass common heater geometries and a shape factor calculated for each geometry by the method described in section 2.1.5.

As previously mentioned, the heater geometry of the torus model is fully described by: resistance wire diameter, d_w; helix inside diameter, d_a; heater outside diameter, d; and pitch, p. These variables were non-dimensionalized in order to reduce the number of curves required to show the results of the computer study. That is, a four dimensional plot was reduced to three dimensions by dividing the heater diameter, helix inside diameter, and pitch by the wire diameter. Therefore, any torus model geometry is described

by three dimensionless variables: the dimensionless diameter, D; the dimensionless helix inside diameter, D_a; and the dimensionless pitch, P.

The results of the study given in Figures (2.4.1), (2.4.2), (2.4.3), and (2.4.4) are presented in terms of the dimensionless variables. Each set of curves is representative of a particular dimensionless pitch. For example, for Figure (2.4.1) the dimensionless pitch is three for any value of dimensionless helix inside diameter or for any value of dimensionless heater diameter. The dimensionless pitch is equal to the stretch ratio of the resistance wire helix from the close wound position to the final position in the finished heater. The stretch ratio for good heater design should be at least three to one to prevent arcing from one turn of the helix to the next. For this reason the dimensionless pitches chosen for the computer study were three, four, five, and eight. The values of the dimensionless helix inside diameters were chosen to include common geometries. The values are 3.5, 6.5, 11, 15.5, 20, 24.5, and 29. Similarly, the dimensionless diameter which is the abscissa on each drawing has a range varying from ten to one hundred. The ordinate for each curve gives the shape factor, G, in inches per inch of axial heater length.

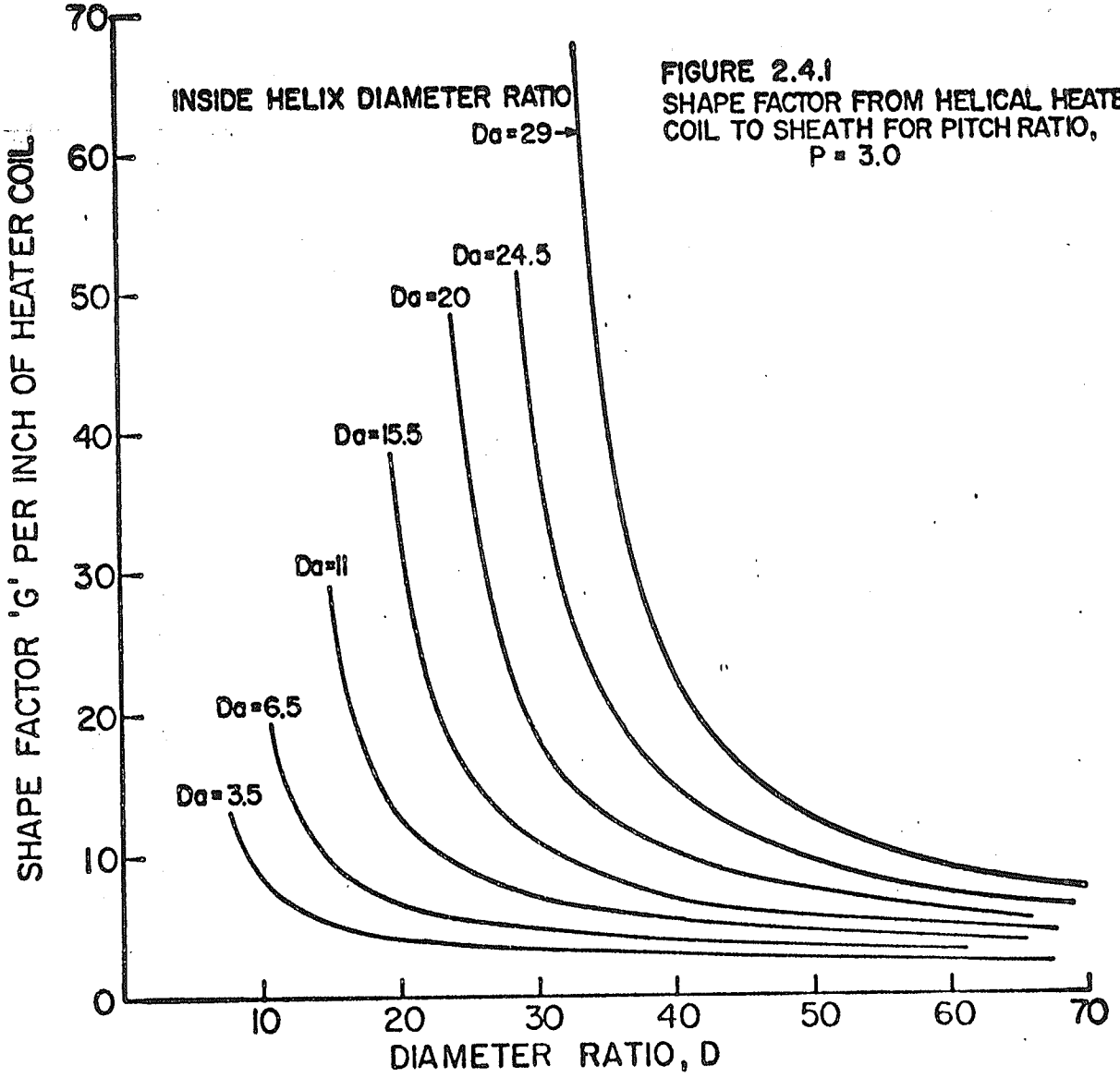

FIGURE 2.4.1
SHAPE FACTOR FROM HELICAL HEATER COIL TO SHEATH FOR PITCH RATIO, P = 3.0

FIGURE 2.4.2
SHAPE FACTOR FROM HELICAL HEATER COIL TO SHEATH FOR PITCH RATIO, P = 4.0

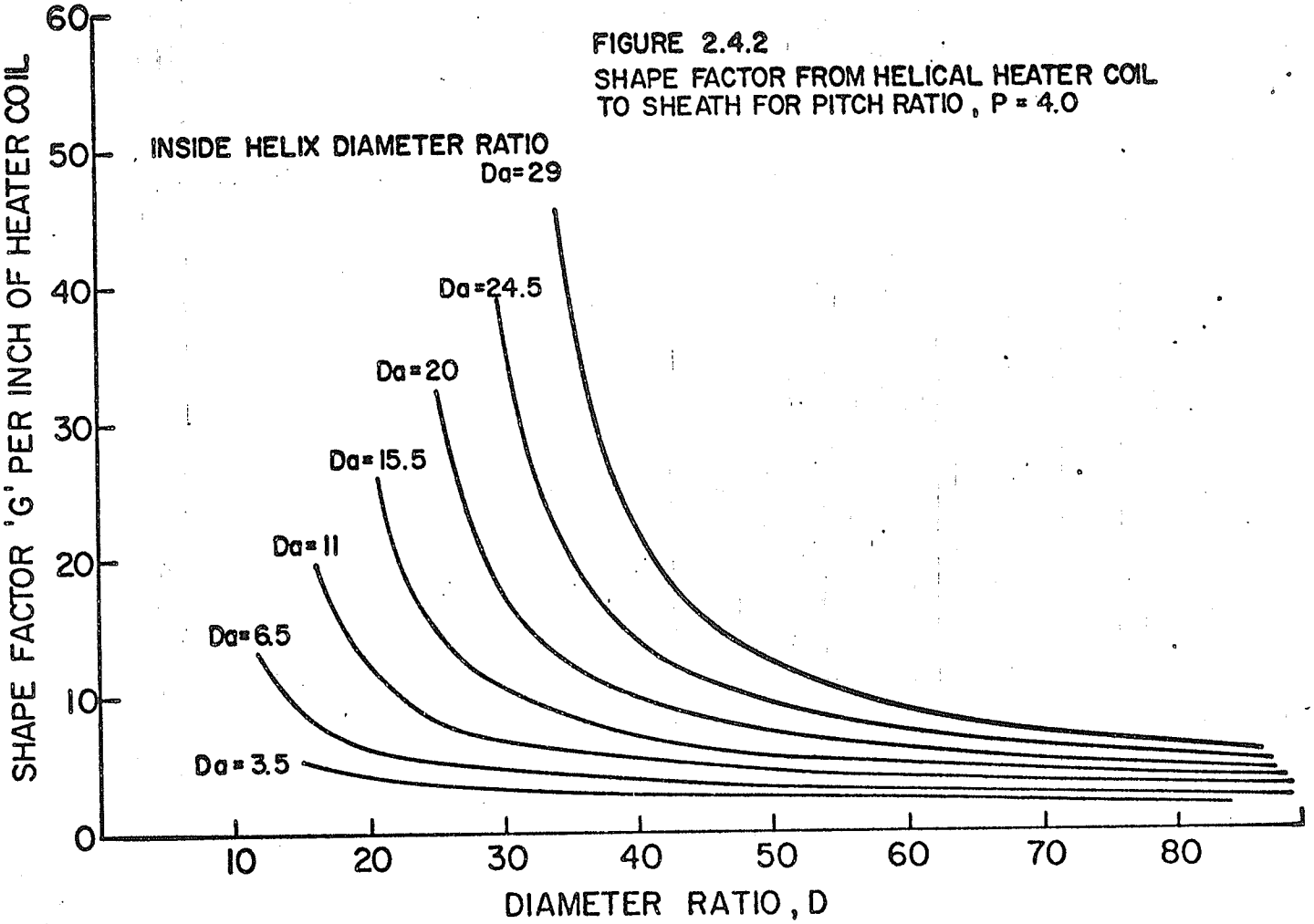

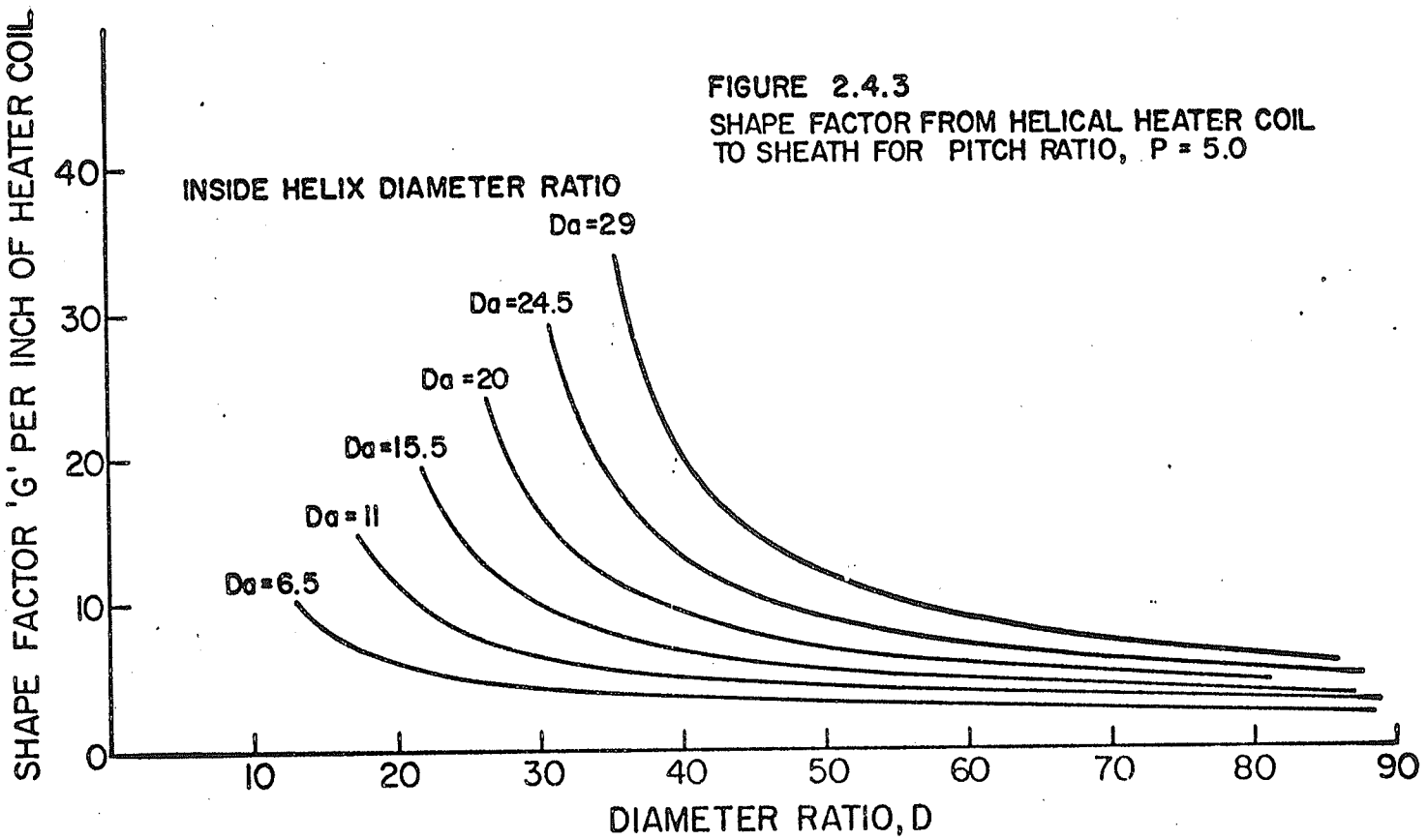

FIGURE 2.4.3
SHAPE FACTOR FROM HELICAL HEATER COIL TO SHEATH FOR PITCH RATIO, P = 5.0

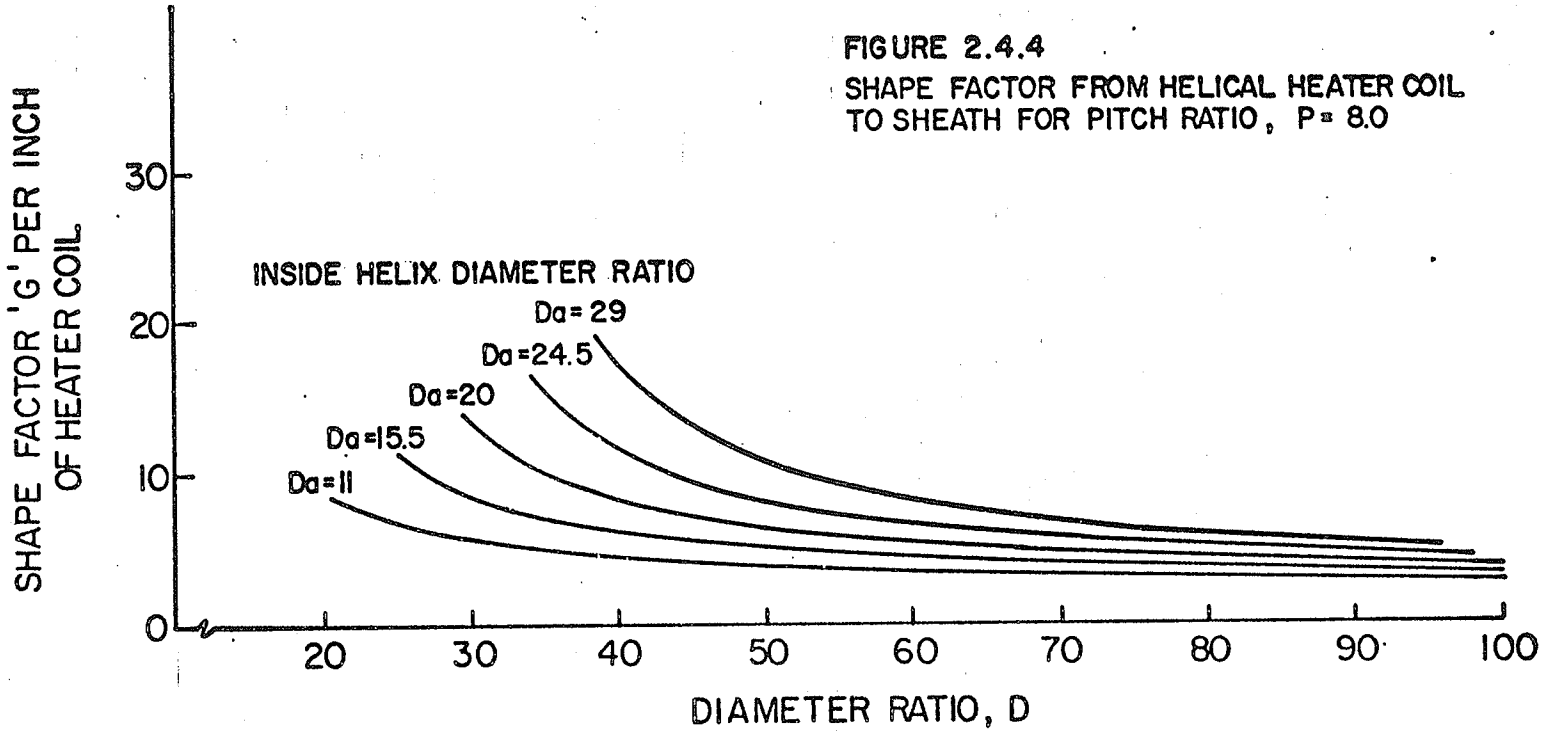

FIGURE 2.4.4
SHAPE FACTOR FROM HELICAL HEATER COIL TO SHEATH FOR PITCH RATIO, P = 8.0

2.2.2 How To Use The Data

The purpose of this study was to make it possible to determine resistance wire temperature for a given watt density and heater geometry. To illustrate the use of shape factors presented in Figures (2.4.1) through (2.4.4) a sample calculation is performed for a real heater.

A baseboard heater is a straight heating element whose surface temperature can easily be measured. In order to calculate the wire temperature the following information must be supplied:

1. wattage
2. axial heated length of the heating element
3. helix inside diameter
4. wire diameter
5. heater diameter
6. pitch
7. heater surface temperature
8. thermal conductance of the insulating material

Once these parameters have been obtained the calculation is straightforward.

First the heat flux per inch axial length of heater is obtained by dividing the wattage by the heated length.

$$Q \text{ (Btu./hr. - inch of heater)} = \frac{\text{Power (watts)} \times 3.414}{\text{heated length (inches)}} \quad \ldots\ldots\ldots \quad 2.4$$

The shape factor must be determined from Figures (2.4.1) through (2.4.4). To do this the geometric variables are non-dimensionalized by the wire diameter. Care must be

exercised when the geometric variables are evaluated. That is, the final helix inside diameter, pitch, and wire diameter must be used since there may be considerable difference in these variables after the element has been roll reduced from what appeared before. This will be discussed in detail in the next section. Once the non-dimensionalized variables have been evaluated the shape factor is chosen from the correct curve. It may be necessary to interpolate or extrapolate between curves or sets of curves.

Knowing the shape factor, the wire temperature is found by rearranging equation 2.1 to read:

$$T_w = \frac{Q}{GK} + T_s \quad \ldots\ldots\ldots \quad 2.5$$

where

T_w = resistance wire temperature (^oF)

T_s = sheath temperature (^oF)

K = thermal conductivity of the electrical insulating material (Btu./hr. - in. - ^oF)

G = shape factor (inch/inch of heater)

Q = heat flux (Btu./hr. - inch of heater)

As a numerical example consider a baseboard heater with the following specifications:

1000 watts
38.5 inches of heated length
0.072 inch helix inside diameter
0.014 inch wire diameter
0.440 inch heater diameter

0.044 inch pitch
400°F heater surface temperature
0.042 Btu./hr. - in. - °F thermal conductance of insulating material

The heat flux per inch of heater is:

$$Q = \frac{1000 \times 3.414}{38.5} = 90.4 \ \frac{\text{Btu.}}{\text{hr. - inch of heater}}$$

Non-dimensionalizing the pitch, helix inside diameter, and heater diameter by dividing by the wire diameter, the non-dimensionalized variables are:

$$P = \frac{0.044}{0.014} = 3.14 \text{ non-dimensional pitch}$$

$$D_a = \frac{0.072}{0.014} = 5.14 \text{ non-dimensional helix inside diameter}$$

$$D = \frac{0.440}{0.014} = 31.4 \text{ non-dimensional heater diameter}$$

Knowing the above parameters, Figures (2.4.1) and (2.4.2) are consulted and by interpolation the shape factor, G is approximately 4.5 inches per inch of heater. Substituting this value into equation 2.5:

$$T_w = \frac{90.4}{4.5 \times 0.042} + 400$$

$$= 878^{\circ}F$$

This is well below the limiting continuous service temperature for tubular resistance heaters.

2.3 Determination of Correct Dimensionless Parameters

The previous section demonstrated how easily the curves in Figures (2.4.1) to (2.4.4) may be used to find a shape factor once the heater geometry is known. However, determining the final geometry in a compacted, straight, tubular heating element is not simple.

Since there are many variables which influence the final geometry, it was impossible to apply a correction to the "as wound helix" that would predict the final geometry in any circumstance. This was mainly due to the process of diameter reduction which occurs after the filling operation. The variations in materials and material properties with the degree of diameter reduction caused by rolling or swaging directly influence the final heater geometry so that it cannot be predicted accurately.

In order to avoid choosing an erroneous shape factor, the correct coil inside diameter, wire diameter, pitch, and heater diameter must be determined from a finished heater. This may be accomplished by carefully cutting the heater apart and measuring or by x-raying the heater against a calibrated transparent grid.

The subsections below describe the variables involved in determining a final geometry and in some cases how these affect the calculation of the correct dimensionless variables.

2.3.1 Springback

As mentioned in section 1.1.2, springback is the elasticity in the resistance wire helix causing it to unwind and increase its inside diameter. That is, as the resistance wire is wound into a helix it undergoes an elastic-plastic deformation. When the constriction holding either end of the helix is removed, it unwinds causing an increase in helix inside diameter. At the same time there are fewer turns of wire in the helix which would be stretched to the same length in the finished heater. Subsequently, there is an increase in pitch over that which might be predicted if the helix inside diameter was assumed to be the arbor diameter. However, while the increase in helix inside diameter causes an increase in shape factor above that predicted at the arbor diameter, the increase in pitch causes the shape factor to decrease beyond that predicted by the original pitch.

In the production of a tubular resistance heater, springback is the first complication that makes the prediction of a final geometry difficult since different wire diameters and types of resistance wire will have different springback characteristics.

An average increase in helix inside diameter due to springback is approximately 0.005 inches. For nearly all cases in real heaters springback will have negligible effect on final geometry.

2.3.2 Sheath Thickness

As was mentioned in section 2.1.2, the sheath material was not modeled as part of the finite element grid. That is, the temperature gradient in the radial direction through the sheath material was assumed negligible. For this reason the dimensionless heater diameter should be calculated as the heater outside diameter minus twice the thickness of the sheath material divided by the resistance wire diameter. That is:

$$D = \frac{d - 2t}{d_w}$$

where

D = dimensionless diameter ratio

d = heater outside diameter (inches)

t = wall thickness of sheath material (inches)

d_w = wire diameter (inches)

This correction becomes more important for small resistance wire diameters and large sheath material thicknesses.

2.3.3 Stretching The Helix

The second process, after springback which complicates the determination of a final geometry in a tubular heater, from the geometry of the helix as wound on the arbor pin, occurs when the helix is stretched during the filling

operation. At this stage in production the helix is fixed at both ends and stretched to the length of the tubing used as sheath material. This causes the helix inside diameter to decrease since the length of resistance wire for one turn of the helix remains constant while pitch increases from one wire diameter in the close wound helix to the larger pitch in the stretched helix.

At this point the helix geometry can be calculated as shown in Appendix A since the original geometry is known and the length of resistance wire for one turn of the helix remains constant. However, this first major change in geometry is further complicated by the next production step as discussed in section 2.3.4

2.3.4 Decrease In Resistance

The third and most unpredictable change in geometry of the resistance wire helix occurs after the tubing used as sheath material is complete with resistance wire helix and filled with granular insulating material such as magnesium oxide. The tubular element is then reduced in outside diameter by passing the tubular sheath through a set of rolls or by the rotary hammering action of a swager. This is done to increase the thermal conductance and electrical resistance of the insulating material and results in elongation of the sheath.

The diameter reduction of the heating element causes a decrease in electrical resistance measured from terminal pin to terminal pin compared to that which existed after the sheath had been filled with insulating material. The decrease in resistance may vary from two per cent to sixty-five per cent and is dependent upon several factors such as: the type and temper of the metal tubing used as sheath material, the original geometry of the resistance wire helix, the fill density of the insulating material achieved inside the sheath during the filling operation, the type of insulating material itself, and the percentage diameter reduction.

There are several possible explanations for this decrease in resistance. One is that high pressures may cause the helix to be pushed into itself and thus thicken the wire causing a decrease in resistance with increasing wire diameter. Another is that several turns of the resistance wire are pushed onto the terminal pin causing a decrease in resistance. Although this seems possible for a two per cent decrease it seems highly improbable for a sixty-five per cent decrease. In fact, x-ray photographs of diameter reduced tubular elements show that this effect is not a large factor. A third possibility is that the electrical resistance of the resistance wire is altered due to metallurgical effects.

2.3.5 Summary

It was not the intent of the author of this thesis to predict the final geometry of a tubular resistance heater which may undergo the above transformations, but rather to solve the conduction heat transfer problem between the resistance wire helix and the metal sheath material. Section 2.3 and the ensuing subsections were included to demonstrate the complicated geometric changes that occur in a tubular resistance heater and to emphasize that care must be exercised in determining; the final wire diameter, pitch, helix inside diameter, and the outside heater diameter minus sheath material. The dimensionless variables are then evaluated and the appropriate shape factor chosen as shown in section 2.2.2.

CHAPTER III

EXPERIMENTAL STUDY

3.1 Electrical Analog

A steady state electrical analog method was used to verify the accuracy of modeling a helix as a series of tori of revolution. In this analog method a series of electrolytic cells which were the geometric equivalents of heater elements were constructed. Appropriate measurements of voltage, current, or resistance were taken so that the shape factor for electrical resistance could be calculated.

In the electrical analog to a conduction heat transfer problem the following parameters are equivalent:

a) The electrical current is equivalent to the heat flux.

b) The voltage gradient is equivalent to the temperature gradient.

c) The electrical resistivity of the electrically conducting liquid is inversely equivalent to the thermal conductivity of the material through which the heat is transferred.

d) The ratio of normal conducting area to path length, the shape factor, is the same for both the electrical analog and the equivalent heat transfer geometry.

The liquid used in this analog method was an ionic conductor or electrolyte. The electrical power source was of high frequency (above 10^3 Hertz) alternating current to negate any electrolytic plating action.

3.2 Experimental Model

This section discusses the theory of the electrical analog as it applies to the particular problem of the helix inside the metal sheath. The physical test apparatus and method is then discussed.

3.2.1 Electrically Conducting Cells

In the electrical analog of a stretched helix inside a tubular metal sheath, the sheath and helix acted as two electrodes at different voltages. The sheath was at a voltage, E_1, which is analogous to a temperature, T_1, while the helix was at a different voltage, E_2, which is analogous to a temperature, T_2. The two electrodes were in electrical contact only through an electrolyte which was sealed inside the sheath. That is, the electrolyte, which in this case was a weak solution of copper sulfate and sulfuric acid, was poured into the sheath around the helix in the same way magnesium oxide would be poured into a real heater. When the cell was connected to a power supply and current flowed across it, Ohm's law states:

$$i = \frac{1}{\rho} \left[\frac{A}{L}\right] \Delta E \qquad \text{.....} \quad (1)$$

where

i = the electrical current (amps)

ρ = the resistivity of the electrolyte (ohms-inch)

ΔE = the potential difference or voltage drop between coil and sheath (volts)

$\frac{A}{L}$ = the shape factor (inch)

and $R = \rho \left[\frac{L}{A}\right]$ ..... (2)

where

R = the total electrical resistance of the cell (ohms)

The conduction heat transfer analog to equations (1) and (2) is:

$Q = K \left[\frac{A}{L}\right] \Delta T$ ..... (3)

where

Q = heat flux (Btu./hr.)

K = thermal conductivity (Btu./hr. - inch - ^{o}F)

ΔT = the temperature difference between coil and sheath (^{o}F)

$\frac{A}{L}$ = the shape factor (inch)

and $R = \frac{1}{K} \left[\frac{L}{A}\right]$ ..... (4)

where

R = the total thermal resistance of the cell $\frac{(^{o}F - hr.)}{Btu.}$

In equation (1) both the resistivity and the shape factor are unknown. In order to experimentally determine the shape factor, a standard with a known shape factor was compared with the unknown helix cell. The standard cell was the concentric cylinder with the inner and outer cylinders

acting as electrodes. The shape factor for this case is:

$$\text{shape factor} = \frac{2\pi L}{\ln (d_o/d_i)} \qquad \ldots\ldots\ldots \quad (5)$$

where

L = length of the cylinder (inches)

d_o = outside diameter of electrolyte -- i.e. inside radius of outer cylinder (inches)

d_i = inside diameter of electrolyte -- i.e. outside radius of inner cylinder (inches)

Since the helix cell and the standard cell could be connected in series, the same current could pass through both. Using the subscript, 1, to indicate the helix cell and the subscript, 2, to indicate the standard cell, equation (1) may be written for each cell as:

$$i = \frac{1}{\rho} (A/L)_1 \Delta E_1 \qquad \ldots\ldots\ldots \quad (6)$$

$$i = \frac{1}{\rho} (A/L)_2 \Delta E_2 \qquad \ldots\ldots\ldots \quad (7)$$

Since the same electrolyte was used in both cells, equation (6) can be divided by equation (7) and rearranged to read:

$$\frac{(A/L)_2}{(A/L)_1} = \Delta E_1/\Delta E_2 \qquad \ldots\ldots\ldots \quad (8)$$

Since the shape factor for the standard cell was known, to find the unknown shape factor, $(A/L)_1$, the ratio of the voltage drops across the two sets of electrodes had to be measured.

Figure (3.1) is a schematic of the electrical analog test method described above.

3.2.2 Use of Alternating Current

The original power source for the circuit shown in Figure (3.1) was a variable voltage direct current power supply. Direct current was used initially to negate any inductive effects in the cell containing the helix. However, the application of direct current proved more difficult than originally anticipated due to problems such as differential electrode areas between the helix cell and the standard cell causing the resistivity of the electrolyte in each cell to be different. Other problems were differential resistance heating of the electrolyte and the formation of concentration gradients within the cells. Many trials of using a direct current power supply for several electrolytes and many applied voltages showed no reproducible results.

The main objection to using alternating current was the inductance effect on the helix cell. To determine the magnitude of the inductive resistance a variable frequency input was connected to the helix cell. An oscilloscope trace showed that there was no significant phase shift of applied alternating current for input frequencies of several kilohertz. Therefore, the inductance was neglected and alternating current equipment was used to measure the circuit shown in Figure (3.1).

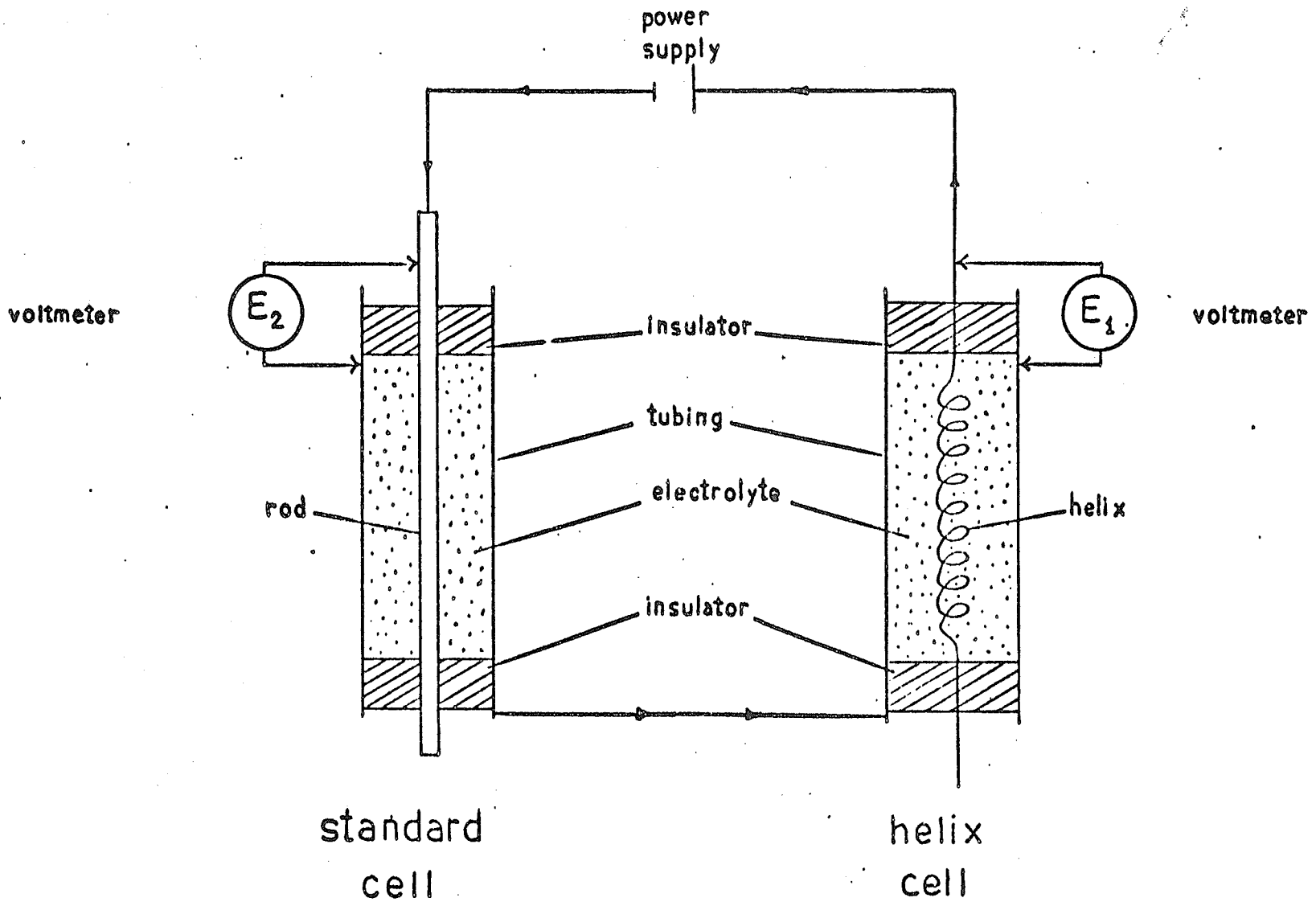

FIGURE 31
SCHEMATIC OF
ELECTRICAL ANALOG

3.2.3 Apparatus

The apparatus used to perform the electrical analog was reduced to four main components when an alternating current source was applied to the circuit; the helix cell, the standard cell, the electrolyte, and the Wayne Kerr B 421 Autobalance Component Bridge. The measurement method employing the Wayne Kerr instrument will be discussed in section 3.2.4.

Figure (3.2) is a photograph of the helix cell. As previously mentioned the outer cylinder and wire helix were both made from commercially pure copper. The two end plugs which electrically insulated the cylinder from the helix were machined from teflon. The plugs also served to hold the helix concentrically with respect to the outer cylinder. The wire helix was threaded onto the bolts shown in the photograph. The threaded washer prevented the bolt from slipping through the teflon plug and into the cell. In this way the washer also served as an adjustment to the stretch ratio of the helix. That is, by turning the washer to the desired position on the bolt a small adjustment could be made to the amount the helix was stretched. The cell was held in a vertical position during testing. Therefore, the bottom teflon plug had to be water-tight to prevent any leakage of electrolyte. This was accomplished by using silicone cement around the periphery of the plug next to the copper cylinder and around the bolt holding the helix. The top plug had two small holes

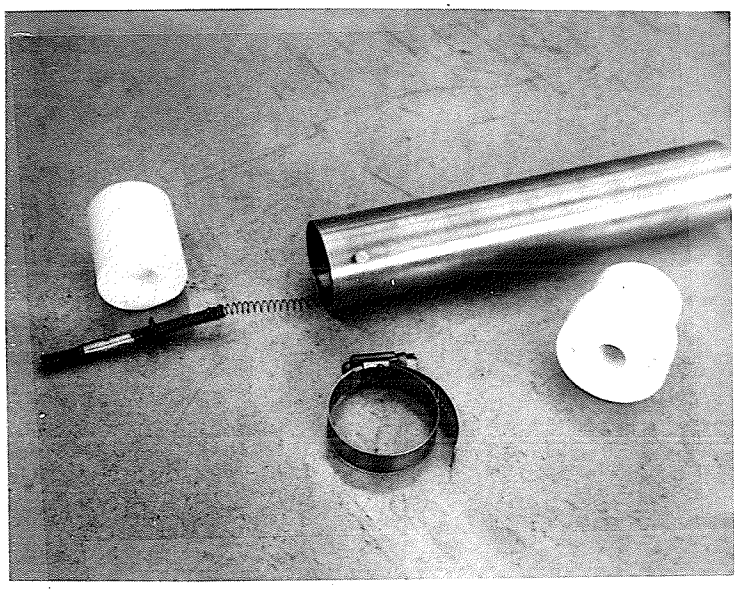

FIGURE 3.2
PHOTOGRAPH OF THE
HELIX CELL

in it beside the larger hole used for the top bolt. These two holes were used to fill the cell with electrolyte once it was assembled with the helix inside. One hole was used to fill the cell and the other acted as an air vent and indicated when the cell was full. The hose clamp around the copper cylinder served to make electrical connection with measuring equipment.

The standard cell was similar to the helix cell in construction. As can be seen in the photograph shown in Figure (3.3) the only difference between the two cells was that no elaborate means for holding the copper rod concentric within the outer copper cylinder was required. The copper rod had a tight fit in the center holes of both teflon plugs.

Figure (3.4) is a photograph of the assembled apparatus ready for test.

3.2.4 Method

The following method was used to determine the shape factor for a particular helix geometry inside an enclosing cylinder.

The copper sulfate, sulfuric acid, and distilled water solution was prepared in a mechanical mixer to ensure that the copper sulfate was completely dissolved. The solution was then strained through filter paper into a clean container ready to be poured into the test cells.

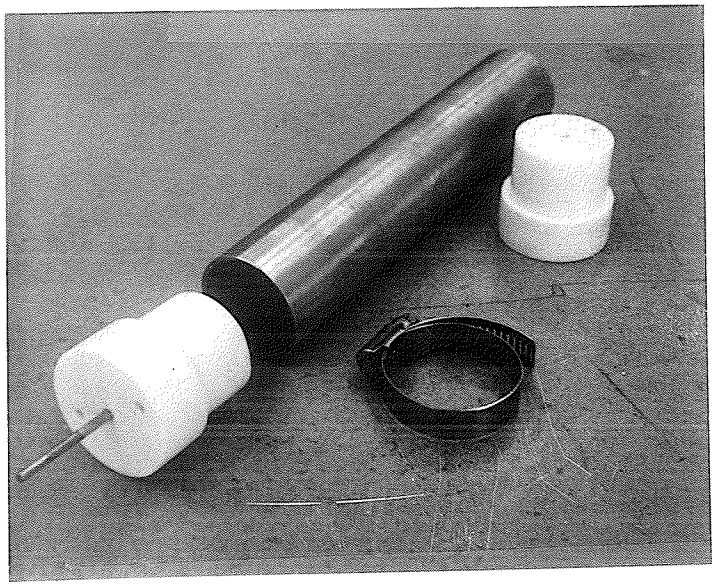

FIGURE 3.3
PHOTOGRAPH OF THE
STANDARD CELL

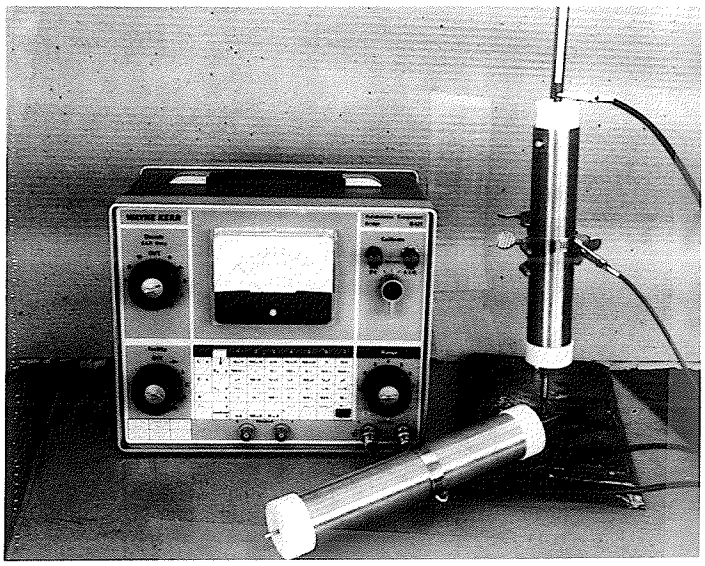

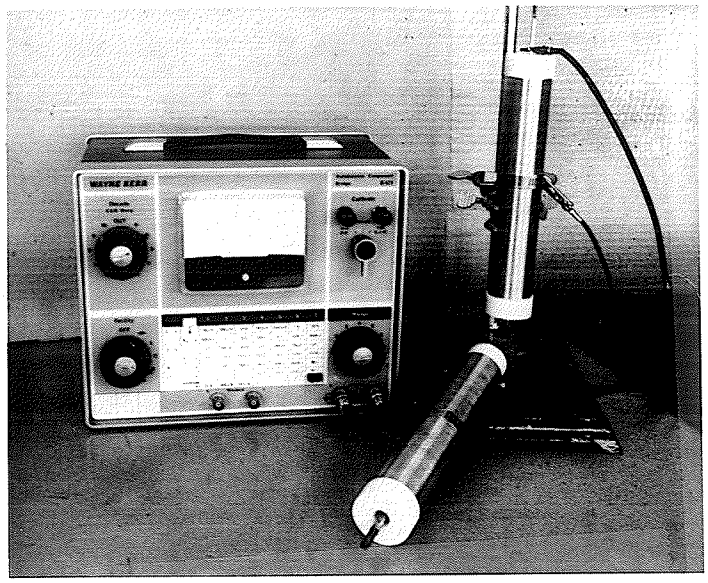

FIGURE 3.4
PHOTOGRAPHS OF THE
ASSEMBLED CELLS
READY FOR TEST

Once the standard cell and the helix cell were sealed to prevent leakage of electrolyte, they were placed in test tube holders and held vertically. The electrolyte was again mixed and then poured into one of the cells through one of the two 0.125 inch holes drilled into the top teflon plug. The other hole acted as an air vent and indicated when the cell was full of electrolyte. The Wayne Kerr B 421 Autobalance Component Bridge was then connected with one lead to each electrode. The lead wires were of heavy gauge copper and as short as possible. They were, therefore, of negligible resistance when compared to the resistance of the cell. The Wayne Kerr Bridge then measured the resistance of the cell being tested. This reading was recorded immediately after the cell was filled with electrolyte (i.e. within one minute) to minimize the effects of any chemical reactions. The remaining cell was then filled with electrolyte poured from the same bottle used to fill the first cell. A resistance measurement was taken and recorded.

As was previously mentioned, no appreciable inductive resistance was found in the helix cell using input frequencies of several kHz. The Wayne Kerr instrument has a bridge frequency of 1 kHz and should, therefore, introduce negligible error due to inductive effects.

This test method deviates somewhat from the method described in section 3.2.1 since the resistance measurement

is made directly and each cell was measured independently. However, the theory of that section still applies and the ratio of cell resistance is equal to the ratio of shape factors since the electrolyte in both cells has the same resistivity and both cells were measured by the same instrument which passes the same current through each cell. Therefore, in equation 3.8 the voltage drop can be replaced by the total resistance of each cell to read:

$$\frac{(A/L)_2}{(A/L)_1} = \frac{R_1}{R_2} \qquad \text{.....} \quad (3.9)$$

where

R_1 = the electrical resistance of the helix cell (ohms)

R_2 = the electrical resistance of the standard cell (ohms)

Only three geometries were tested due to the difficulty in obtaining uncoated copper wire to use for helix construction. Also, the apparatus did not allow a wide variety of geometries to be tested since the tube inside diameter (which is equivalent to the heater outside diameter) was fixed, as was the diameter of the threaded connection which held the helix concentric inside the tube.

3.3 Presentation of Data

Three different helix geometries were tested using the method described in section 3.2.4. Each geometry was tested

three times using a different helix and batch of electrolyte on each trial. Table 3.2 shows the results of the tests and the percentage deviation of these results from those predicted by the theoretical analysis given in Chapter II. A discussion of these discrepencies is presented in the next chapter.

In order to predict the ratio of helix cell shape factor to the standard cell shape factor, the shape factor per unit axial length (per inch) of the standard cell must be calculated. Since the standard cell was a concentric cylinder, equation 3.5 gives the shape factor as:

$$G_{std} = \frac{2\pi L}{\ln (d_o / d_i)} = 2.529 \text{ inches} \quad \ldots\ldots\ldots\ldots (3.10)$$

where

G_{std} = standard cell shape factor

L = 1.00 inches

d_o = 1.50 inches

d_i = 0.125 inches

The helix cell shape factor, G, per unit axial length was established by interpolation of the original data obtained from the analytical analysis which was used to plot the curves in Figures (2.4.1) through (2.4.4). The dimensionless parameters used were those found by dividing the helix geometry given in the extreme left hand column of Table 3.1 by the wire diameter.

TABLE 3.1

RESULTS OF THE EXPERIMENTAL STUDY

* Helix Cell Geometry Inches	Trial Number	Standard Cell Resistance, R_2 Ohms	Helix Cell Resistance, R_1 Ohms	$\frac{R_2}{R_1}$	$\frac{R_2}{R_1}$ Predicted by Theoretical Analysis	** % Difference between Experimental and Theoretical Analysis
p = 0.096 d_w = 0.032 d_a = 0.218 d = 1.50	1 2 3	3.07 3.17 3.89	2.24 2.14 2.76	1.37 1.48 1.41	1.42	- 3.5 + 4.3 - 0.7
p = 0.096 d_w = 0.032 d_a = 0.125 d = 1.50	1 2 3	4.67 4.75 4.80	3.89 4.46 4.50	1.20 1.07 1.07	1.14	+ 5.3 - 6.1 - 6.1
p = 0.160 d_w = 0.032 d_a = 0.234 d = 1.50	1 2 3	3.60 3.72 3.17	2.44 2.51 2.14	1.47 1.48 1.48	1.39	+ 5.7 + 6.4 + 6.4

* p = helix pitch

d_w = wire diameter

d_a = helix inside diameter

d = heater outside diameter

** based on theoretical analysis

Having obtained the analytical value of the helix shape factor which was modeled as a series of tori, the theoretical ratio of G/G_{std} is easily calculated. For example, using the first geometry the dimensionless parameters are:

$$P = 3.00$$

$$D_a = 6.81$$

$$D = 46.9$$

By interpolation of the original data, the corresponding shape factor per inch axial length of helix is 3.60 inches.

The ratio G/G_{std} is, therefore:

$$\frac{G}{G_{std}} = \frac{3.60}{2.529} = 1.42$$

It is this value which appears in the sixth column in Table 3.1. This is the ratio predicted by the analytical model presented in Chapter II. This ratio is compared to the experimental results shown in the fifth column, with the percentage difference based on the analytical analysis shown in the seventh column. As stated in equation 3.9, the ratio of the shape factors is inversely equal to the ratio of the total cell resistances. That is:

$$\frac{G}{G_{std}} = \frac{R_2}{R_1} \qquad \text{.....} \quad (3.11)$$

Similar calculations were performed on the other two geometries.

CHAPTER IV

DISCUSSION

4.1 Error Analysis

This section contains a discussion of the systematic and random errors that occurred in the experimental model and their effects on the ratio of the helix cell shape factor to the standard cell shape factor.

The percentage difference between the ratio of the helix cell shape factor to the standard cell shape factor predicted by the theoretical analysis of Chapter II and that predicted by the experimental model of Chapter III are shown in Table 3.1. The average percentage difference based on three trials of each of the three geometries tested was: 2.8 per cent for the first geometry, 5.8 per cent for the second geometry, and 6.2 per cent for the third geometry. The possible causes of these discrepancies are presented below.

4.1.1 Error Analysis Of The Apparatus

The following is an error analysis of the effect of the uncertainty in the geometric variables on the standard cell and helix cell shape factors. Instrument error is also included. The analysis was made following the format and theory of a single sample experiment as was presented by Kline

and McClintock (ref. 4). The detailed analysis appears in Appendix B.

The analysis showed that the uncertainty in the geometric variables associated with the helix cell contributed negligible percentage error to the helix cell shape factor. This was especially true when compared to the percentage difference between the average shape factor ratio, G/G_{std}, found by experiment and that predicted by the theoretical analysis of Chapter II. The small error was primarily due to the fact that the change in the helix cell shape factor was not greatly affected by small variations in the dimensionless variables in the range of the geometries tested. However, for small values of the dimensionless diameter and large values of the dimensionless helix inside diameter (see Figures (2.4.1) through (2.4.4), the change in shape factor with small variations in the dimensionless variables could become significant.

The error analysis of the instrumentation was easily obtained since the only instrument used was the Wayne Kerr B 421 autobalance component bridge. The manufacturer states an uncertainty in each reading of $\pm$ 0.25 per cent of full scale. Again this was considered negligible when compared with the difference between experimental and theoretical values of the shape factor ratio.

The error analysis of the effect of uncertainty in the

geometric variables on the shape factor for the standard, concentric cylinder cell is also shown in detail in Appendix B. The percentage error in the shape factor was estimated as 1.7 per cent and while still not responsible for all of the difference between the experimental and theoretical shape factor ratios was still considered significant.

4.1.2 Systematic Errors

When predicting the theoretical helix cell shape factor, two systematic errors were introduced.

The first error was due to assuming that the diameter of the arbor pin on which the helix was wound was also the inside diameter of the stretched helix as it appeared in the helix cell. This was not actually the case since the helix inside diameter increases due to springback and then decreases when the helix is stretched from its close wound condition, as was explained in section 2.3. The magnitude of the error introduced by assuming the arbor pin diameter to be the helix inside diameter was determined by applying the method shown in Appendix A. A springback allowance of 0.005 inches was used. The worst error occurred in the second geometry tested where the nominal helix inside diameter was 0.125 inches and the calculated diameter was 0.127 inches. This was a percentage difference of 1.6 per cent, but, however, caused a negligible difference in the shape factor. In each geometry

the calculated value of the helix inside diameter was slightly higher than the mean value used. This would imply an even less significant increase in the helix cell shape factor. The nominal diameter of the arbor pin was taken as the mean value for error analysis because the helix inside diameter was the only geometric variable that could not be easily measured by means of calipers.

The second systematic error was caused by modelling the helix as a series of tori of revolution and assuming that the real helix would behave exactly the same as the torus model. The main difference between the two models is that there is a longer length of wire in one turn of the helix than for the equivalent torus of revolution. Therefore, there is more surface area available for heat transfer in the helix than in the torus model. The percentage difference between the area of one turn in the helix and the area of one equivalent torus was calculated as: 2.0 per cent for the first geometry, 3.3 per cent for the second geometry, and 1.9 per cent for the third geometry. As a very rough approximation, the larger percentage area could be assumed to cause a corresponding percentage increase in the helix cell shape factor. If the measured shape factor ratio was higher than that predicted by the theoretical analysis then the difference could be explained by this difference in surface area plus the error in the standard cell geometry. However, as can be seen in

Table 3.1 this is not the case. For example, in the second geometry, which has the largest differential in area between the helix and the torus model, two of the three trials show that ratio of the helix cell shape factor to the standard cell shape factor was lower than that predicted by the theoretical analysis. The first geometry shows a similar scatter of the results. The third geometry showed that every trial produced a shape factor ratio that was higher than that predicted by theory in all three trials. However, the ratio was higher than could be explained by the sum of the increased surface area effect and the standard cell geometric error.

4.1.3 Undefined Errors

Sections 4.1.1 and 4.1.2 showed that the discrepancies between the shape factor ratio found experimentally and that predicted theoretically could not be fully explained by the uncertainty in geometric variables, instrument error, or errors inherent in modelling the helix as a series of tori of revolution. Therefore, another undefined error must exist. One possibility is contaminated electrodes which would cause an increase in cell resistance in either the helix cell or the standard cell. Another possibility is that the resistivity

of the electrolyte in one cell may have been slightly different than the resistivity of the electrolyte in the other cell. Since no measurements were made of these two effects (although precautions were taken to minimize any possible effects), their magnitude remains unknown.

The effect of eccentricity on the standard cell shape factor was also investigated. It was found that in the geometries tested, a relatively large degree of eccentricity caused a negligible change in the standard, concentric cylinder cell shape factor. For example, a 0.050 inch eccentricity caused only a 1.0 per cent difference in shape factors. Therefore, eccentricity was not considered as a major possible source of error.

Despite the differences between the shape factor ratios predicted analytically and those found experimentally, an excellent correlation existed between the two results. The Chi-Square goodness of fit test indicated a 0.99 probability or greater that the experimental data matched the analytical predictions when the least probable set of data was examined. The test was performed by considering each helix cell geometry separately. The shape factor ratio of each trial in that geometry was considered a discreet observation and was compared to the ratio predicted analytically. The analytical ratio was considered the mean value. The only restriction in freedom was that of the number of observations.

4.2 Torus Model Versus An Actual Tubular Heating Element

As was mentioned in section 4.1.2 an error exists when the torus model is assumed to be the exact equivalent of a resistance wire helix. The torus model becomes a poor approximation to the real helix in two instances.

In the first case, a small value of the dimensionless helix inside diameter, Da, combined with a large value of the dimensionless pitch, P, will cause a large difference between the length of wire required to make one torus as was modelled in the computer program and the length of wire required for one turn of the actual helix. The magnitude of this effect can be calculated using the method shown in Appendix A. For example, consider the helix geometry having an original close wound helix inside diameter of 0.072 inches made from a resistance wire of 0.040 inches in diameter. If the helix is stretched to three times its original length, the surface area available for heat transfer in the real helix would be 5.9 per cent greater than that predicted by the torus model. If, however, this same geometry was stretched to eight times its original length the difference in areas would be 57 per cent and the theoretical model would collapse.

The second instance in which the torus model becomes

a poor approximation to a real heater occurs when the helix outside diameter is very close to the heater outside diameter. That is for large values of the dimensionless inside helix diameter, Da, combined with small values of the dimensionless heater diameter, D. In this case the torus model collapses because the outside surface of the heater was assumed isothermal in the axial direction during the computer analysis.

Fortunately, common heater geometries do not contain either of the above geometrical configurations. Therefore, the torus model is an accurate model of the helix contained within an actual heater for most heater geometries and the shape factors presented in Figures (2.4.1) through (2.4.4) can be used in the conduction equation 2.1 to compute resistance wire temperature.

CHAPTER V

CONCLUSION

5.1 Statement Of Accomplishment

The main accomplishment of this thesis was determining the effect of the geometric variables present in a tubular resistance heater on the conduction heat transfer between the resistance wire helix and the tubular metal sheath. Within the limitation of the design variables, a designer can quantitatively compare one heater geometry to another and choose the most advantageous design.

If the thermal conductivity of the magnesium oxide insulation is known or can be approximated, then the operating temperature of the resistance wire can be calculated by the method shown in Chapter II. The designer could then determine whether or not an excessive wire temperature will promote premature failure of the heating element.

5.2 Suggestions For Further Study

The major uncertainty in solving the conduction equation for heat transfer in tubular resistance heaters is the value of thermal conductivity of magnesium oxide, the electrical insulating material used to separate the resistance wire helix from the metal sheath. Present literature only

discusses the thermal conductivity on a qualitative basis. It is known to be a strong function of both density and temperature and to a lesser extent also of grain size. This is one area that requires further study.

Some further work could be done on expanding the number of geometries tested using the electrical analog technique developed in Chapter III. For example, due to lack of time and available apparatus no geometries were tested that had large values of the dimensionless helix inside diameter coupled with small values of the dimensionless heater diameter.

One other task that could be undertaken would be to develop an equation to fit the theoretical data shown as curves in Figures (2.4.1) through (2.4.4).

APPENDIX A

CALCULATION OF CHANGE IN HELIX INSIDE DIAMETER UPON STRETCHING FROM CLOSE WOUND TO FINAL PITCH

In order to calculate the change in arbor diameter with increasing pitch consider first the helix in its close wound position. Figure (A-1) illustrates the helix as it would appear if its cylindrical shape were cut axially, unwrapped, and shown in two dimensions. The subscript, 1, indicates the conditions that exist when the helix is close wound. The length of one turn of the helix is shown as a line inclined at the helix lead angle. The line represents the axial center line of the resistance wire which would be wound on a mean diameter which is the sum of the helix inside diameter and one wire diameter (if springback is neglected). The circumference of the mean diameter is shown in Figure (A-1) as; $(d_{a_1} + d_w)\,\pi$. From the geometry the length of one turn of resistance wire can be calculated as:

$$\ell = \frac{(d_{a_1} + d_w)\,\pi}{\cos \theta_1} \qquad \text{..... (1)}$$

where

$$\theta_1 = \tan^{-1} \frac{d_w}{\pi\,(d_{a_1} + d_w)} \qquad \text{..... (2)}$$

and

ℓ = length of resistance wire for one turn of the helix

d_{a_1} = helix inside diameter at the close wound position

d_w = resistance wire diameter

θ_1 = helix lead angle at the close wound position

the length, l, is constant for any pitch and it is also assumed that the resistance wire cross sectional area does not change.

Figure (A-2) shows the helix in two dimensions after it has been stretched to a new pitch. The subscript, 2, indicates the new condition. The pitch may easily be calculated since the number of turns of resistance wire in the helix is constant and the length to which the helix is stretched is known. That is, the new pitch is:

$$\text{pitch} = \frac{\text{helix length}}{\text{number of turns of resistance wire}}$$

The length for one turn of the helix is already known, therefore, the new helix inside diameter is found from the geometry as:

$$d_{a_2} = \frac{p}{\pi \tan \theta_2} - d_w$$

where

$$\theta_2 = \sin^{-1} \frac{p}{\ell}$$

and

p = pitch

d_{a_2} = helix inside diameter at the stretched position

θ_2 = helix lead angle at the stretched position

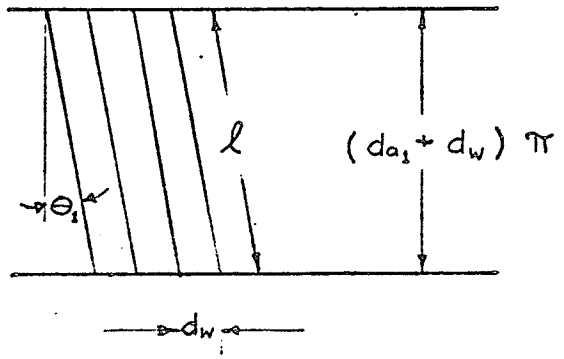

FIGURE A-1

CLOSE WOUND HELIX

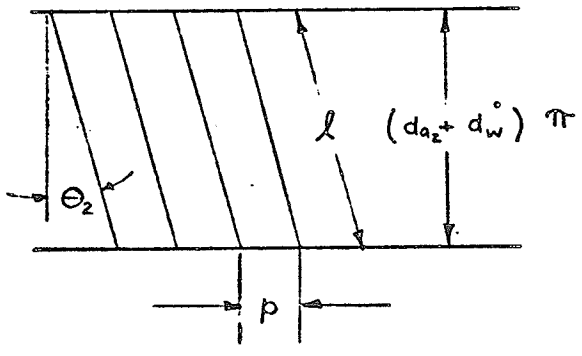

FIGURE A-2

STRETCHED HELIX

APPENDIX B

ERROR ANALYSIS OF EXPERIMENTAL DATA

Since there were an insufficient number of observations made to do a comprehensive statistical analysis of experimental error, the error analysis was made on a single sample basis proposed by Kline and McClintock, (ref. 4). Using their terminology and nomenclature, the uncertainty in each variable was specified as a mean of the readings and an uncertainty interval based on specified odds. That is:

$$m \pm \omega \quad \text{(b to 1)}$$

where

m = arithmetic mean of observed values

ω = uncertainty interval

b = the odds

Kline and McClintock defined a result, R, as a function of variables; $\nu_1, \nu_2, \nu_3, \ldots\ldots\ldots \nu_n$. Each variable, ν_i, had an uncertainty interval, ω_i, based on certain odds. The uncertainty in the result, ω_R, is then related to the uncertainty in the variables as follows:

$$\omega_R = \left[\left[\frac{\partial R}{\partial V_1} \omega_1 \right]^2 + \left[\frac{\partial R}{\partial V_2} \omega_2 \right]^2 + \ldots + \left[\frac{\partial R}{\partial V_n} \omega_n \right]^2 \right]^{\frac{1}{2}} \quad \ldots(1)$$

The odds expressed for each uncertainty interval was a measure of the confidence the experimenter had that any reading

would lie within its estimated uncertainty interval. For this error analysis odds of twenty to one were chosen for the uncertainty interval in each variable.

The subsections that follow give an error analysis of the helix cell, the standard concentric cylinder cell, and the total error in ratio of the helix cell shape factor to the standard cell shape factor including instrument error.

Error Analysis Of The Helix Cell

In this subsection the effect of the uncertainty in geometric variables on the helix cell shape factor is analyzed. The geometric variables are; the pitch, p; the helix inside diameter, d_a; the heater outside diameter, d; and the wire diameter, d_w. In order to determine a shape factor from the data compiled in the computer study these four variables were non-dimensionalized as shown in Chapter III to read:

$$P = \frac{p}{d_w} \qquad \ldots\ldots\ldots \qquad (2)$$

$$D_a = \frac{d_a}{d_w} \qquad \ldots\ldots\ldots \qquad (3)$$

$$D = \frac{d}{d_w} \qquad \ldots\ldots\ldots \qquad (4)$$

The uncertainty in each of the non-dimensionalized variables from equation (1) is:

$$\omega_P = \left[\left[\frac{\partial P}{\partial p} \omega_p \right]^2 + \left[\frac{\partial P}{\partial d_w} \omega_{d_w} \right]^2 \right]^{\frac{1}{2}} \quad \ldots\ldots\ldots \quad (5)$$

$$\omega_{D_a} = \left[\left[\frac{\partial D_a}{\partial d_a} \omega_{d_a} \right]^2 + \left[\frac{\partial D_a}{\partial d_w} \omega_{d_w} \right]^2 \right]^{\frac{1}{2}} \quad \ldots\ldots\ldots \quad (6)$$

$$\omega_D = \left[\left[\frac{\partial D}{\partial d} \omega_d \right]^2 + \left[\frac{\partial D}{\partial d_w} \omega_{d_w} \right]^2 \right]^{\frac{1}{2}} \quad \ldots\ldots\ldots \quad (7)$$

To simplify equations (5), (6), and (7) the differentiation was performed and equations (5), (6), and (7) were divided by equations (2), (3), and (4) respectively to read:

$$\frac{\omega_P}{P} = \left[\left[\frac{\omega_p}{p} \right]^2 + \left[\frac{\omega_{d_w}}{d_w} \right]^2 \right]^{\frac{1}{2}} \quad \ldots\ldots\ldots \quad (8)$$

$$\frac{\omega_{D_a}}{D_a} = \left[\left[\frac{\omega_{d_a}}{d_a} \right]^2 + \left[\frac{\omega_{d_w}}{d_w} \right]^2 \right]^{\frac{1}{2}} \quad \ldots\ldots\ldots \quad (9)$$

$$\frac{\omega_D}{D} = \left[\left[\frac{\omega_d}{d} \right]^2 + \left[\frac{\omega_{d_w}}{d_w} \right]^2 \right]^{\frac{1}{2}} \quad \ldots\ldots\ldots \quad (10)$$

Having determined the uncertainty intervals of the non-dimensionalized variables, the uncertainty in the shape factor, G, from equation (1) is:

$$\omega_G = \left[\left[\frac{\partial G}{\partial P} \omega_P \right]^2 + \left[\frac{\partial G}{\partial D_a} \omega_{D_a} \right]^2 + \left[\frac{\partial G}{\partial D} \omega_D \right]^2 \right]^{\frac{1}{2}} \ldots \quad (11)$$

In equation (11) the uncertainties in the dimensionless variables are found from equations (8), (9), (10). The terms $\frac{\partial G}{\partial P}$, $\frac{\partial G}{\partial D_a}$, and $\frac{\partial G}{\partial D}$ have values which must be determined from the computer data since the analytical relationship between G and the non-dimensionalized variables is unknown.

In the geometries tested the uncertainties in the geometric variables contributed negligible error to the helix cell shape factor. This is best illustrated by an example. The first geometry tested had the following mean values and uncertainty intervals:

$p = 0.096" \pm 0.002"$

$d_a = 0.218" \pm 0.005"$

$d = 1.50" \pm 0.005"$

$d_w = 0.032" \pm 0.0002"$

The corresponding mean values of the non-dimensionalized variables are:

$$P = \frac{p}{d_w} = 3.00$$

$$D_a = \frac{d_a}{d_w} = 6.81$$

$$D = \frac{d}{d_w} = 46.9$$

The percentage uncertainties in the non-dimensionalized variables are found by substituting the appropriate variables into equations (8), (9), and (10). Putting in the numbers:

$$\frac{\omega_P}{P} = \left[(4.34 \times 10^{-4}) + (3.91 \times 10^{-5})\right]^{\frac{1}{2}} = \pm 2.16\%$$

$$\frac{\omega_{D_a}}{D_a} = \left[(5.26 \times 10^{-4}) + (3.91 \times 10^{-5})\right]^{\frac{1}{2}} = \pm 2.38\%$$

$$\frac{\omega_D}{D} = \left[(1.11 \times 10^{-5}) + (3.91 \times 10^{-5})\right]^{\frac{1}{2}} = \pm 0.709\%$$

The corresponding non-dimensional uncertainty interval are, therefore:

$$\omega_P = \pm 0.0648$$

$$\omega_{D_a} = \pm 0.162$$

$$\omega_D = \pm 0.0110$$

Finally, to determine the uncertainty in the helix cell shape factor, G, the following quantities were found from the original tabulated data using the appropriate uncertainty interval; ω_P, ω_{D_a}, or ω_D:

$$\frac{\partial G}{\partial P} = \pm 0.0042 \quad \text{(inches/inch of heater)}$$

$$\frac{\partial G}{\partial D_a} = \pm 0.044 \quad \text{(inches/inch of heater)}$$

$$\frac{\partial G}{\partial D} \simeq 0 \quad \text{(inches/inch of heater)}$$

Substituting the above values into equation (11), the uncertainty interval for the shape factor is:

$$\omega_G = \{\{(0.0042)\ (0.0648)\}^2 + \{(0.044)\ (0.162)\}^2 + \{0\}^2\}^{\frac{1}{2}} = \pm 0.0071$$

The mean value of G from the original tabulated data was 3.60 inches/inch of heater. Therefore, the percentage uncertainty is:

$$\frac{\omega_G}{G} = \pm 0.20\%$$

This error was considered to be negligible when compared with those found in other parts of the experiment.

The other two geometries tested have similar uncertainties which have negligible effect on the shape factor.

Error Analysis Of The Standard Cell

In this subsection the effect of the uncertainty in geometric variables on the standard cell shape factor will be analyzed. Since the standard cell was a concentric cylinder, the shape factor is related to the geometric variables by:

$$G_{std} = \frac{2\pi L}{\ln (d_o / d_i)} \qquad \ldots\ldots\ldots\ldots (12)$$

where

G_{std} = the standard cell shape factor

L = the axial length of the cell

d_o = the inside diameter of the copper tubing which corresponds to the outside diameter of the concentric cylinder cell

d_i = the outside diameter of the copper rod which was placed concentrically inside the tubing

Equation (1) was used to determine the uncertainty in the standard cell shape factor due to the geometric variables, L, d_o, and d_i as follows:

$$\omega_{G_{std}} = \left[\left[\frac{\partial G_{std}}{\partial L} \omega_L \right]^2 + \left[\frac{\partial G_{std}}{\partial d_i} \omega_{d_i} \right]^2 + \left[\frac{\partial G_{std}}{\partial d_o} \omega_{d_o} \right]^2 \right]^{\frac{1}{2}} \ldots\ldots (13)$$

To simplify equation (13) the differentiation was performed and equation (13) was divided by equation (12) to read:

$$\frac{\omega_{G_{std}}}{G_{std}} = \left[\left[\frac{\omega_L}{L}\right]^2 + \left[\frac{\omega_{d_i}}{d_i \ln(d_o/d_i)}\right]^2 + \left[\frac{\omega_{d_o}}{d_o \ln(d_o/d_i)}\right]^2\right]^{\frac{1}{2}} \quad \ldots\ldots \quad (14)$$

The following mean values and uncertainty intervals were substituted into the non-dimensionalized equation (14).

$L = 6.00 \pm 0.030$ (inches)

$d_o = 1.50 \pm 0.005$ (inches)

$d_i = 0.125 \pm 0.005$ (inches)

Substituting the above values into equation (14), the percentage uncertainty in the standard cell shape factor due to the uncertainty in the geometric variables was:

$$\frac{\omega_{G_{std}}}{G_{std}} = \left[(2.5 \times 10^{-5}) + (2.59 \times 10^{-4}) + (1.80 \times 10^{-6})\right]^{\frac{1}{2}} = \pm 1.7\%$$

Although this error is small relative to the difference between the expected and observed values of the experimental data it is considerably larger than the error introduced by geometric variable in the helix cell shape factor.

Instrument Error

The only measurement taken was the total resistance measurement on the Wayne Kerr B 421 Autobalance component

bridge. The manufacturer states an uncertainty interval of $\pm$ 0.25 per cent of full scale reading on the range being used. Therefore, the mean value and the uncertainty for the instrument used for the experiment is:

$$10 \pm 0.025 \quad \text{(ohms)}$$

Again the instrument error was considered negligible when compared with other discrepancies in the experiment.

Error In The Ratio Of The Helix Cell To The Standard Cell Shape Factor

Taking into account the instrument error and the error in geometric variables in both the helix and the standard cell, the total percentage uncertainty in the ratio of the helix cell shape factor to the standard cell shape factor according to equation (1) is:

$$\frac{\omega_R}{R} = \left[\left[\frac{\omega_G}{G} \right]^2 + \left[\frac{\omega_{G_{std}}}{G_{std}} \right]^2 \right]^{\frac{1}{2}} \qquad \text{..... (15)}$$

where

$$R = \frac{G}{G_{std}}$$

For an example, using the first geometry tested, where G had a mean value of 3.60 inches per inch of heater, the total percentage error in the ratio of the shape factor was $\pm$ 1.75 per cent. Again this shows that instrument error and the

error in the geometry of the helix cell had negligible effect on the ratio of the shape factors when compared to the error caused by the uncertainty in the geometry of the standard concentric cylinder cell.

REFERENCES

1. F. S. Epstein, "Coil Temperature Measurement By The Change In Resistance Method". A paper presented At The Fifth Magnesium Oxide Symposium, Toronto, Ontario, February 17, 1966.

2. T. R. Hsu; G. A. Bertels; B. Arya; and S. Banerjee, "Application Of The Finite Element Method To The Nonlinear Analysis Of Nuclear Reactor Fuel Behaviour". Computational Methods In Nonlinear Mechanics - Editor: J. T. Oden, Texas Institute For Computational Mechanics, pp. 531-540. 1974.

3. E. L. Wilson and R. E. Nickell, "Application Of The Finite Element Method To Heat Conduction Analysis", Nuclear Engineering and Design, Vol. 4, pp. 276-286. 1966.

4. S. J. Kline and F. A. McClintock, "Describing Uncertainties In Single-Sample Experiments", Mechanical Engineering Journal, pp. 3-8. January, 1953.

5. J. P. Holman, "Experimental Methods For Engineers", McGraw Hill Book Company, New York, New York. 1966.

6. H. D. Young, "Statistical Treatment Of Experimental Data", McGraw Hill Book Company, New York, New York, 1962.

7. G. A. Hawkins and M. Jakob, "Elements Of Heat Transfer", Third Edition, J. Wiley & Sons, New York, New York. 1966.